https://doi.org/10.5194/egusphere-2025-4910
Preprint. Discussion started: 13 November 2025

Improving Simulation of Earth System Variability through Weakly Coupled Ocean Data Assimilation in E3SM

Pengfei Shi[1,*], L. Ruby Leung[1,*], Zhaoxia Pu[2], Samson Hagos[1], and Karthik Balaguru[1]

[1] *Atmospheric, Climate, and Earth Sciences Division, Pacific Northwest National Laboratory, Richland, Washington, USA*

[2] *Department of Atmospheric Sciences, University of Utah, Salt Lake City, Utah, USA*

[*] To whom correspondence may be addressed. Pengfei Shi (pengfei.shi@pnnl.gov) and L. Ruby Leung (Ruby.Leung@pnnl.gov)

https://doi.org/10.5194/egusphere-2025-4910
Preprint. Discussion started: 13 November 2025

Abstract. Accurate initialization of ocean states is essential for skillful prediction of Earth system variability across seasonal to decadal timescales. In this study, we evaluate the impact of a newly developed four-dimensional ensemble variational (4DEnVar)-based weakly coupled ocean data assimilation (WCODA) system within the DOE Energy Exascale Earth System Model version 2 (E3SMv2) on global and regional climate variability. By assimilating monthly ocean temperature and salinity from the EN4.2.1 reanalysis into the fully coupled model, we demonstrate substantial improvements in simulating both interannual and decadal climate variability. Compared to the free-running coupled simulation, the assimilation experiment exhibits markedly enhanced interannual correlations with observations for global mean surface air temperature and precipitation anomalies. The representation of key climate modes, including ENSO, the Indian Ocean Dipole, and multidecadal variability in the Pacific and Atlantic Oceans, also improves significantly. Regional evaluation over the contiguous United States further shows enhanced skill in simulating winter surface air temperature and precipitation variability, particularly in the northern and southern regions, respectively, linked to improved ENSO representation. These findings underscore the critical role of coupled forecasts in the data assimilation cycle for propagating observational information across Earth system components. By integrating ocean observations within a coupled framework, the WCODA system enables cross-component information exchange among the ocean, atmosphere, and land, thereby generating physically consistent initial states. These improvements contribute to more accurate simulations of Earth system variability across multiple timescales and advance the development of more reliable prediction systems in support of societal resilience.

https://doi.org/10.5194/egusphere-2025-4910
Preprint. Discussion started: 13 November 2025

1. Introduction

Accurately representing climate variability across multiple timescales remains a major challenge in climate modeling and prediction. The initial conditions (ICs) of the climate system, including the ocean, atmosphere, and land surface, play a crucial role in determining the accuracy and reliability of climate predictions (Boer et al., 2016; Taylor et al., 2012). Among these components, the ocean exhibits the longest memory and exerts a dominant influence on climate variability through its interactions with the atmosphere and other components (Wang, 2019). Therefore, improving the initialization of ocean states has been widely recognized as a key approach for enhancing the skill of seasonal to decadal climate predictions (Meehl et al., 2021; Zhu et al., 2017).

Data assimilation (DA) methods have been developed to integrate observational data into coupled models, thereby improving the ICs and enhancing predictive skill. Traditionally, ocean DA has been conducted in an uncoupled framework, where ocean observations are assimilated into a standalone ocean model forced by prescribed atmospheric forcings (Carton and Giese, 2008). The resulting ocean analyses are then combined with the optimal analyses from other uncoupled components (e.g., atmosphere and land) to generate the ICs for coupled models. However, because each component is initialized independently, this uncoupled approach often leads to inconsistencies and imbalances among the different components, potentially introducing initial shocks that degrade coupled model forecasts (Mulholland et al., 2015; Zhang, 2011). To address these limitations, recent studies have increasingly employed coupled data assimilation (CDA) (Wu et al., 2018; Zhang et al., 2012).

CDA has emerged as an advanced framework for performing ocean DA directly within the coupled model. CDA methods are generally categorized into weakly coupled data assimilation (WCDA) and strongly coupled data assimilation (SCDA). In WCDA, ocean observations are assimilated separately into the ocean component during the analysis step, but the coupled model is utilized in the forecast step to transfer ocean observational information to other components through multi-component interactions (Browne et al., 2019). The key difference between WCDA and uncoupled DA lies in whether a coupled model is employed to generate the background forecast: WCDA uses a coupled model during the forecast step but assimilates

https://doi.org/10.5194/egusphere-2025-4910
Preprint. Discussion started: 13 November 2025

observations independently within each component, whereas uncoupled DA employs separate component models throughout the entire assimilation cycle (Shi et al., 2024a; Zhang et al., 2020). Unlike uncoupled DA, CDA can produce more balanced and self-consistent ICs and thus enhance forecast skill (Feng et al., 2018; Shi et al., 2022). However, WCDA does not account for cross-component background error covariances during the analysis step, limiting its ability to explicitly correct coupled state errors (Tang et al., 2021). In contrast, SCDA incorporates cross-component background error covariances during the analysis step, enabling observations in one component to instantaneously update the state variables of other components (Penny et al., 2019; Lin and Pu, 2020). By treating the coupled system as an integrated whole, SCDA offers the potential for more pronounced assimilation improvements over WCDA (Han et al., 2013; Sluka et al., 2016; Lin and Pu, 2019). However, the practical implementation of SCDA faces considerable challenges owing to the difficulty of estimating cross-component error statistics, and consequently, WCDA remains more widely adopted in current systems (Zhou et al., 2024).

The Energy Exascale Earth System Model (E3SM) is a state-of-the-art Earth system model developed by the U.S. Department of Energy to advance the understanding of Earth system variability and change (Leung et al., 2020). Recently, Shi et al. (2025) developed a new weakly coupled ocean data assimilation (WCODA) system for E3SMv2 utilizing the four-dimensional ensemble variational (4DEnVar) method. Despite this advancement, the impacts of this 4DEnVar-based WCODA system on simulating climate variability have not yet been systematically assessed. The objective of this study is to evaluate the influence of the E3SM coupled ocean data assimilation on the simulation of climate variability across global and regional scales. Specifically, the evaluation focuses on four key aspects: (1) surface air temperature and precipitation anomalies over ocean, land, and global domains; (2) major tropical variability modes, including the Indian Ocean Dipole (IOD) and El Niño-Southern Oscillation (ENSO); (3) decadal-to-multidecadal variability modes, such as the Pacific Decadal Oscillation (PDO), Interdecadal Pacific Oscillation (IPO), and Atlantic Multidecadal Oscillation (AMO); and (4) regional climate variability over the contiguous United States.

The paper is structured as follows. Section 2 describes the E3SMv2 model, datasets, and

https://doi.org/10.5194/egusphere-2025-4910
Preprint. Discussion started: 13 November 2025

experimental design. Section 3 presents the results from analyzing major modes of climate variability. Finally, the conclusions and discussion are provided in Section 4.

2. Model, data and experimental design

2.1 Model description

E3SMv2 is a fully coupled Earth system model that includes the atmospheric, ocean, sea ice, land and river transport components. The atmospheric component (EAMv2) is based on a spectral-element dynamical core with 72 vertical levels and is configured on a cubed-sphere grid with approximately 110 km horizontal resolution (Golaz et al., 2022). The ocean component (MPAS-O) employs an unstructured Voronoi mesh with horizontal spacing of ~60 km in the midlatitudes and ~30 km near the equator and poles, and includes 60 vertical layers using a z-star coordinate (Reckinger et al., 2015). The sea ice component (MPAS-SI) shares the same horizontal mesh with MPAS-O and provides detailed representations of sea ice thermodynamics and dynamics (Turner et al., 2022). The land component (ELMv2) simulates land surface energy and water fluxes, biophysical processes, and soil hydrological processes (Golaz et al., 2019). The river transport component (MOSARTv2) represents streamflow routing across river basins (Li et al., 2013). These five components are dynamically coupled through the CPL7 coupler, which facilitates the exchange of momentum, heat, and mass fluxes among model components (Craig et al., 2012). The detailed description and assessment of E3SMv2 can be found in Golaz et al. (2022).

2.2 Datasets

Three types of monthly reanalysis datasets are used for evaluation: 1) ERA5 reanalysis data, including surface air temperature, 850 hPa winds, and 500 hPa geopotential height. ERA5 incorporates a wide range of satellite and in situ observations to produce high-quality global atmospheric fields (Hersbach et al., 2020). 2) Global Precipitation Climatology Project (GPCP) monthly precipitation data. This dataset provides reliable global precipitation estimates based on satellite microwave, infrared measurements, and surface rain gauge data (Adler et al., 2003). 3) Hadley Centre Sea Ice and Sea Surface Temperature (HadISST) data. HadISST offers

https://doi.org/10.5194/egusphere-2025-4910
Preprint. Discussion started: 13 November 2025

monthly sea surface temperature (SST) analysis derived from a combination of in situ measurements and satellite-based retrievals (Rayner et al., 2003).

2.3 Data assimilation scheme

The 4DEnVar method employed in the WCODA system is based on the dimension-reduced projection four-dimensional variational (DRP-4DVar) algorithm (Wang et al., 2010). In DRP-4DVar, the ensemble-based approach is used to replace the adjoint model traditionally required in standard 4DVar, thereby significantly reducing computational cost. The DRP-4DVar method determines the optimal state in the ensemble subspace by fitting observational data to model-generated ensemble samples within a four-dimensional assimilation window (Liu et al., 2011; Shi et al., 2021). Due to its flexibility and efficiency, this method has been widely applied in diverse numerical models to improve the initialization of ocean, land, and atmospheric states (He et al., 2020; Shi et al., 2024b; Zhu et al., 2022).

In this study, monthly mean ocean temperature and salinity from the EN4.2.1 reanalysis (Good et al., 2013) are assimilated into the ocean component of the fully coupled E3SMv2 model within a one-month assimilation window. Each monthly assimilation cycle consists of the analysis and forecast stages. First, the fully coupled E3SMv2 model is run forward for one month using the background ICs to generate model-derived monthly means of ocean temperature and salinity. In the analysis stage, the differences between these model outputs and the EN4.2.1 reanalysis are calculated to form the observational innovation. The DRP-4DVar scheme then applies this innovation to compute the optimal ICs for the ocean component at the beginning of the assimilation cycle. During the following forecast stage, the fully coupled model is rewound to the start of the month and re-integrated for the same month using the optimized ocean state and the background fields from other components. Through this coupled forecast, ocean observational information is dynamically propagated to influence the state variables of other components (e.g., atmosphere and land) through multi-component interactions. Thus, while assimilation is confined to the ocean, employing the fully coupled E3SMv2 model in the forecast stage enables the transfer of assimilated ocean information to other Earth system components, classifying this system as a WCDA framework (Zhang et al.,

https://doi.org/10.5194/egusphere-2025-4910
Preprint. Discussion started: 13 November 2025

2020). Further technical details of the assimilation system are described in Shi et al. (2025).

2.4 Numerical experiments

Two numerical experiments are conducted to assess the impact of the WCODA system on climate variability: a control experiment (CTRL) and an assimilation experiment (ASSIM). In the CTRL experiment, the fully coupled E3SMv2 model is integrated freely from 1950 to 2021 under observed historical external forcings. This experiment serves as the reference for evaluating the influence of the assimilation system. In contrast, the ASSIM experiment assimilates monthly mean ocean temperature and salinity from the EN4.2.1 reanalysis into all 60 layers of the ocean component in the fully coupled E3SMv2 model from 1950 to 2021 using a one-month assimilation window. Considering sparse observational coverage and large uncertainties, the Arctic Ocean is excluded from the assimilation process. At the beginning of each month, monthly mean ocean temperature and salinity from the EN4.2.1 reanalysis are assimilated to update the ocean ICs, after which the fully coupled model is integrated freely until the end of the month. During this forecast period, the assimilated ocean information is dynamically propagated to other components through multi-component interactions. Both CTRL and ASSIM experiments are forced with the same historical external forcings prescribed by the CMIP6 protocol (Eyring et al., 2016).

3. Results

3.1 Surface air temperature and precipitation

The temporal evolution of detrended annual mean surface air temperature anomalies over ocean, land, and global domains is shown in Fig. 1. Compared to CTRL, ASSIM better captures the interannual variability of observed temperature in all three domains. Over the ocean, the correlation coefficient between ASSIM and observation reaches 0.47, much higher than that of CTRL (0.09). Over land and global domains, the correlation coefficients for ASSIM are 0.44 and 0.49, respectively, both of which also exceed those from CTRL (land/global: 0.26/0.18). All three correlations from ASSIM pass the 95% confidence level, indicating significant improvements in simulating observed temperature variability. These results highlight the

https://doi.org/10.5194/egusphere-2025-4910
Preprint. Discussion started: 13 November 2025

effectiveness of ocean data assimilation in enhancing the simulation of interannual temperature variability. The improvement is particularly notable over the ocean, where the assimilated ocean state exerts a direct influence on near-surface atmospheric conditions. Over land, the increased correlations suggest that the benefits of ocean data assimilation extend beyond oceanic regions, reflecting its broader influence on enhancing simulations of interannual temperature variability across all domains.

Figure 2 displays the spatial distribution of climatological mean differences in surface air temperature. Compared to observations, CTRL exhibits widespread cold biases over the tropical and subtropical oceans, as well as notable warm biases at high latitudes. In contrast, these biases are significantly reduced in ASSIM, particularly over the North Pacific, North Atlantic, and the midlatitude Southern Ocean. Specifically, the cold bias in the North Pacific decreases from -1.81 °C in CTRL to -0.76 °C in ASSIM, and from -3.23 °C to -1.09 °C in the North Atlantic. The warm bias over the midlatitude Southern Ocean is notably reduced from 1.07 °C in CTRL to 0.13 °C in ASSIM. Improvements are also evident over land regions, such as eastern China, northern Eurasia, northern Africa, and parts of North America. The spatial pattern of reduced surface air temperature bias closely aligns with the reduction in SST bias reported by Shi et al. (2025), underscoring the critical role of realistic ocean states in shaping near-surface temperature patterns.

The interannual variability of detrended precipitation anomalies over ocean, land, and global domains is illustrated in Fig. 3. Compared to CTRL, ASSIM shows markedly improved agreement with observed interannual precipitation variability across all three domains. Over the ocean, the correlation with observations increases from 0.11 in CTRL to 0.52 in ASSIM, while over land it improves from 0.27 to 0.60. At the global scale, the correlation rises from 0.04 in CTRL to 0.55 in ASSIM. All three correlations from ASSIM are statistically significant at the 95% confidence level. These results suggest that assimilating observed ocean states enhances the simulation of interannual precipitation variability over both ocean and land, with the latter improvement possibly related to atmospheric circulation and moisture transport. Notably, the relatively high correlations for both surface air temperature (0.26) and precipitation (0.27) over land in CTRL suggest some influence of external forcing on land

https://doi.org/10.5194/egusphere-2025-4910
Preprint. Discussion started: 13 November 2025

surface climate variability.

Figure 4 shows the spatial distribution of climatological mean precipitation and associated model biases. In the observation (Fig. 4a), major precipitation maxima are located along the Intertropical Convergence Zone (ITCZ) in the equatorial Pacific, the South Pacific Convergence Zone (SPCZ) extending northwest–southeast from the western Pacific, and the tropical Indian Ocean. A dry zone is also evident along the west coast of South America. Compared to observations, CTRL overestimates precipitation over the central Pacific and the southern equatorial Atlantic, while significantly underestimating rainfall over the tropical eastern Indian Ocean and the northern equatorial Atlantic (Figs. 4b & d). In contrast, these biases are substantially reduced in ASSIM (Figs. 4c & e). Precipitation in the tropical eastern Indian Ocean is enhanced, improving agreement with observations. Moreover, in the tropical Atlantic, the dry bias over the northern equatorial Atlantic is reduced from -1.27 mm/day in CTRL to -0.34 mm/day in ASSIM, while the wet bias over the southern equatorial Atlantic decreases from 1.81 mm/day to 0.62 mm/day.

3.2 ENSO

ENSO is the dominant mode of interannual climate variability in the tropics and exerts profound impacts on global atmospheric circulation (Chiang and Sobel, 2002). ENSO variability is commonly monitored by the Niño 3.4 index, defined as the SST anomalies averaged over the equatorial central Pacific (5°S–5°N, 120°W–170°W) (Trenberth and Stepaniak, 2001). To evaluate the representation of ENSO variability, we analyze the time evolutions of the monthly and winter Niño 3.4 index (Fig. 5). As expected, CTRL exhibits very weak correlations with observations, with correlation coefficients of only 0.02 for the monthly and 0.07 for the winter Niño 3.4 index, indicating the model's limited ability to reproduce the evolution of tropical SST variability in the absence of observational constraints. Compared with CTRL, ASSIM exhibits substantial improvements in simulating ENSO variability. The temporal evolution of the Niño 3.4 index in ASSIM closely matches the observation, with correlations increasing to 0.87 for the monthly and 0.95 for the winter index. These results underscore the critical role of ocean data assimilation in constraining tropical Pacific SST

https://doi.org/10.5194/egusphere-2025-4910
Preprint. Discussion started: 13 November 2025

variability and enhancing ENSO representation in coupled models.

Figure 6 further evaluates ENSO characteristics through the power spectra and seasonal cycle of the monthly Niño 3.4 index. The observed spectrum exhibits a pronounced peak in the 3–5 year band, consistent with typical ENSO periodicities (Fig. 6a). This spectral feature is reasonably well reproduced in ASSIM (Fig. 6b). By comparison, CTRL underestimates the variance in this band and produces an unrealistically amplified peak at 2–3 years (Fig. 6c). Beyond its frequency characteristics, ENSO also exhibits a strong seasonal cycle. The observed Niño 3.4 index shows minimum variance in April and peak amplitude in December, reflecting the well-known phase-locking behavior of ENSO (Fig. 6d). ASSIM capture this seasonal cycle well, although the minimum occurs one month later (Fig. 6e). In contrast, CTRL exhibits a flatter seasonal cycle with markedly weaker variance during the winter peak, and its seasonal minimum is delayed by two months (Fig. 6f).

To further assess the representation of ENSO-related atmospheric variability, we examine the Southern Oscillation Index (SOI), which reflects the east–west seesaw pattern in sea level pressure (SLP) between the western and eastern tropical Pacific. The SOI is commonly defined as the normalized difference in SLP anomalies between Tahiti and Darwin, and serves as the atmospheric counterpart to the Niño 3.4 index (Hanley et al., 2003). Figure 7 presents the temporal evolution of the monthly and winter SOI from the observation, ASSIM, and CTRL. The observed SOI exhibits pronounced interannual fluctuations associated with ENSO phases. Consistent with its poor simulation of the Niño 3.4 index, CTRL fails to capture the observed SOI variability, with correlations of -0.02 for the monthly and -0.04 for the winter index. In contrast, ASSIM reproduces the SOI variability more realistically, with correlations increasing to 0.40 for the monthly and 0.62 for the winter index. These improvements indicate that assimilating observed ocean states not only constrains SST but also improves the representation of ENSO-related atmospheric circulation anomalies in coupled models.

3.3 IOD

The Indian Ocean Dipole (IOD) is a prominent mode of interannual variability in the tropical Indian Ocean that strongly influences surrounding climate systems (Saji et al., 2006).

https://doi.org/10.5194/egusphere-2025-4910
Preprint. Discussion started: 13 November 2025

It typically begins to develop in boreal summer and reaches its peak during autumn. A widely used metric for quantifying IOD variability is the Dipole Mode Index (DMI), defined as the difference in SST anomalies between the western (50°E–70°E, 10°S–10°N) and eastern (90°E–110°E, 0°–10°S) equatorial Indian Ocean (Saji et al., 1999). The temporal evolution of the autumn DMI is further shown in Fig. 8. The observed DMI exhibits pronounced interannual variations associated with alternating positive and negative IOD phases. The CTRL simulation substantially overestimates the IOD amplitude and shows a weak correlation of -0.11 with observations. Such overestimation is the common bias in coupled climate models, as noted in previous studies (Ju et al., 2025). In contrast, ASSIM shows notable improvements in both the amplitude and temporal variability of the DMI, with the correlation increasing to 0.56 and exceeding the 95% confidence level. These results highlight the benefits of ocean data assimilation for improving the simulation of IOD variability.

3.4 PDO, IPO, AMO

The Pacific Decadal Oscillation (PDO) is the leading mode of decadal SST variability in the North Pacific, characterized by basin-scale SST anomalies that typically persist for one to two decades. The PDO index is derived as the leading empirical orthogonal function (EOF) mode of detrended SST anomalies over the North Pacific (20°–70°N, 110°E–100°W) (Mantua et al., 1997). Figure 9 illustrates both the temporal evolution and spatial pattern of the annual PDO index from 1965 to 2016. The observed PDO index displays a canonical sequence of phase transitions: a cool phase before the late 1970s, a persistent warm phase extending into the late 1990s, and a return to negative values thereafter (Fig. 9a). These decadal transitions are reasonably captured by ASSIM, yielding a temporal correlation of 0.67 with observations (Fig. 9b). In contrast, CTRL fails to reproduce the observed phase transitions, with a much lower correlation of 0.19 (Fig. 9c). Besides the temporal evolution, the spatial structure of the PDO index is also analyzed. The observed pattern exhibits a horseshoe-shaped structure with cold anomalies in the central North Pacific and warm anomalies along the western coast of North America (Fig. 9d). This spatial pattern is well reproduced in ASSIM, with a spatial correlation of 0.90 (Fig. 9e). However, the PDO pattern from CTRL exhibits a distorted

https://doi.org/10.5194/egusphere-2025-4910
Preprint. Discussion started: 13 November 2025

structure, and its spatial correlation decreases to 0.68 (Fig. 9f). These improvements in both the temporal evolution and spatial structure of the PDO underscore the potential of the assimilation system to enable more skillful decadal climate predictions by providing improved initial states.

Beyond the North Pacific, another major mode of decadal variability affecting the entire Pacific basin is the Interdecadal Pacific Oscillation (IPO). Similar to the PDO, the IPO index is obtained from the leading EOF mode of detrended SST anomalies, but computed over the whole Pacific (50°S–50°N, 100°E–70°W) (Doblas-Reyes et al., 2013). The annual evolution of the IPO index is shown in Fig. 10, indicating the basin-wide coherence of Pacific decadal variability. The observed IPO index undergoes distinct decadal shifts, including a negative phase prior to the late 1970s, a prolonged positive phase extending through the 1980s and 1990s, and a return to negative values in the early 2000s. These phase transitions are closely reproduced by ASSIM, which achieves a high temporal correlation of 0.80 with observations. On the other hand, CTRL fails to track the decadal evolution of the observed IPO and shows a much weaker correlation of 0.20. These results highlight the importance of ocean data assimilation in constraining Pacific-basin SST variability on decadal timescales and enhancing the representation of long-term Pacific climate variability.

In addition to the Pacific, the North Atlantic also exhibits notable low-frequency SST variability characterized by the Atlantic Multidecadal Oscillation (AMO). The AMO index is computed as the linearly detrended SST anomalies averaged over the North Atlantic (0–60°N, 0–80°W) (Enfield et al., 2001). Figure 11 presents the temporal evolution of the annual AMO index from 1965 to 2016. The observed AMO index shows a pronounced negative phase in the 1970s and 1980s, followed by a persistent positive phase beginning in the mid-1990s. These phase transitions are more accurately reproduced in ASSIM than in CTRL, particularly the timing and amplitude of the warm shift after the mid-1990s. The temporal correlation with observations is 0.71 in ASSIM, much higher than 0.17 in CTRL. The enhanced representation of AMO phases in ASSIM reinforces its potential for better predicting related climate impacts over the North Atlantic and adjacent regions.

3.5 U.S. T2m and Precipitation

Building on the improved representation of tropical SST variability through ocean data assimilation, we extend our analysis to assess its impact on regional climate over land. Given the well-established influence of ENSO on U.S. winter climate variability (Ropelewski and Halpert, 1986; Higgins et al., 2000), we evaluate model performance in simulating interannual temperature and precipitation variability over the contiguous U.S. during boreal winter (Figs. 12 & 13). For winter surface air temperature (Fig. 12), ASSIM exhibits widespread increases in temporal correlation with observations across large portions of the northern and western U.S., particularly over the Intermountain West and Great Lakes regions. In these areas, correlation improvements commonly exceed 0.3 and locally surpass 0.4. Consistent with the correlation patterns, RMSE reductions in ASSIM are also evident across the northern and central U.S., with maximum decreases up to 0.6 °C over the central Great Plains.

In contrast to temperature, improvements in winter precipitation simulations are more localized but remain pronounced across the southern U.S. (Fig. 13). Compared with CTRL, ASSIM shows higher correlations with observed precipitation over the Southwest, southern Great Plains, and Southeast. In particular, significant enhancements are evident in parts of California, Texas, and Alabama, where correlation increases exceed 0.4 and locally approach 0.5. These correlation improvements are accompanied by consistent reductions in RMSE across similar regions. Notably, the largest RMSE reductions, exceeding 0.45 mm/day, are found over coastal California. The spatial coherence of these improvements highlights the critical role of realistic ocean states in better capturing land precipitation variability.

To further investigate the mechanisms underlying the improved simulation of U.S. winter climate, we examine the regression of surface air temperature and precipitation onto the Niño 3.4 index during boreal winter (Fig. 14). The observed patterns reveal that ENSO exerts a pronounced influence on U.S. winter climate through large-scale atmospheric responses. During El Niño events, positive geopotential height anomalies dominate the northern part of the continent, which may suppress the southward intrusion of cold air masses. This circulation pattern could lead to anomalous warming across the northern U.S., producing significant positive correlations with ENSO in these regions (Fig. 14a). Meanwhile, strengthened

https://doi.org/10.5194/egusphere-2025-4910
Preprint. Discussion started: 13 November 2025

subtropical westerlies enhance moisture transport into the southern U.S., favoring increased precipitation and yielding strong positive correlations with ENSO across the southern tier of the country (Fig. 14d).

These ENSO-related spatial structures are well reproduced in ASSIM (Figs. 14b & e). In particular, the regression patterns of temperature and precipitation in ASSIM closely resemble those in the observations, especially across the northern and southern U.S., respectively. Moreover, the regions with robust ENSO-related signals in ASSIM largely overlap with areas showing improved correlation and reduced RMSE in Figs. 12 and 13, suggesting that enhanced representation of ENSO variability may underpin its superior performance in simulating U.S. winter climate. In contrast, CTRL exhibits notable deviations from the observed ENSO-related patterns, especially in the spatial distribution of temperature responses (Figs. 14c & f). These results underscore the importance of accurate ENSO representation for improving simulations of U.S. winter climate variability.

4 Conclusions

Accurate representation of climate variability across multiple timescales is essential for enhancing the reliability of Earth system predictions. One key factor influencing climate variability is the ocean state, owing to its long memory and strong coupling with the atmosphere. While ocean data assimilation has proven effective in improving the simulation of ocean conditions, many existing systems remain uncoupled and thus have limited ability to support coupled forecasts due to imbalances among model components (Mulholland et al., 2015; Zhang et al., 2011). To address this limitation, Shi et al. (2025) recently developed a new 4DEnVar-based WCODA system for E3SMv2 that enables direct assimilation of ocean observations within a coupled model framework. Despite this progress, the extent to which the WCODA system improves simulations of global and regional climate variability has not been fully assessed. This study aims to systematically evaluate its impacts on simulating major modes of climate variability and regional climate over the U.S., demonstrating its potential to enhance initialization and predictive capabilities in coupled Earth system models.

Our results show that the WCODA system significantly improves the representation of

https://doi.org/10.5194/egusphere-2025-4910
Preprint. Discussion started: 13 November 2025

both interannual and decadal climate variability. Significant enhancements are achieved in capturing interannual variability and reducing model biases of surface air temperature and precipitation over land and ocean domains. Notably, the temporal evolution of major climate modes, including ENSO, IOD, PDO, IPO, and AMO, is markedly improved. Besides better capturing the temporal evolution of various modes, assimilating ocean temperature and salinity also improves the seasonal and interannual variability of ENSO and the spatial pattern of PDO over the North Pacific. Furthermore, regional evaluations over the contiguous U.S. reveal increased skill in reproducing the observed interannual variability of winter surface air temperature in the northern U.S. and precipitation in the southern regions, respectively. The improved simulation of U.S. winter temperature and precipitation is closely associated with enhanced ENSO representation, as indicated by spatially coherent regression patterns between Niño 3.4 and U.S. winter climate. These findings demonstrate the capability of the WCODA system to deliver more skillful simulations of Earth system variability through improved ocean initial states and cross-component information exchange.

Despite these promising results, several limitations remain and offer opportunities for future development. The current assimilation system does not incorporate atmospheric or sea ice observations, which may limit its ability to fully constrain coupled model states. Moreover, the WCODA framework is implemented as a weakly coupled system and does not explicitly consider cross-component background error covariances during the analysis stage. Transitioning towards a strongly coupled ocean data assimilation would further improve the accuracy and physical consistency of initial states. Looking ahead, the WCODA system provides a promising foundation for improving the initialization of large-ensemble hindcast experiments from seasonal to decadal timescales. Future work will also leverage these experiments to systematically assess the impact of accurate ocean initial states on the predictability of climate variability and extreme events. These efforts will have important implications for advancing seamless climate prediction and informing risk management in energy and water systems.

Code and data availability. The E3SMv2 source code is freely available under an open-source license and can be accessed via Zenodo at https://zenodo.org/records/16652680. The ERA5 reanalysis datasets are accessible from the Copernicus Climate Change Service through the Climate Data Store portal: https://cds.climate.copernicus.eu/datasets/reanalysis-era5-single-levels-monthly-means?tab=download (Hersbach et al., 2020). Monthly GPCP precipitation data can be obtained from https://psl.noaa.gov/data/gridded/data.gpcp.html (Adler et al., 2003). HadISST sea surface temperature data are available at https://www.metoffice.gov.uk/hadobs/hadisst (Rayner et al., 2003) and EN4.2.1 ocean temperature and salinity data can be accessed from https://www.metoffice.gov.uk/hadobs/en4 (Good et al., 2013). Model outputs are available on Zenodo at https://zenodo.org/records/16740831.

Author contributions. PS and LRL designed the experiments. PS developed the ocean data assimilation system and performed the model simulations. PS and LRL analyzed the results. PS and LRL drafted the initial manuscript. ZP, SH, and KB contributed to manuscript revisions.

Competing interests. The authors declare no competing interests.

Acknowledgements. This research was supported by the Office of Science, Department of Energy Biological and Environmental Research (BER) as part of the Water Cycle: Modeling of Circulation, Convection, and Earth System Mechanisms (WACCEM) Scientific Focus Area funded by the Regional and Global Model Analysis program area. Pacific Northwest National Laboratory is operated by Battelle Memorial Institute for the U.S. Department of Energy under contract DE-AC05-76RL01830. This research used computing resources of the National Energy Research Scientific Computing Center, which is supported by the Office of Science of the U.S. Department of Energy under Contract No. DE-AC02-05CH11231, and the BER Earth and Environmental System Modeling program's Compy computing cluster located at Pacific Northwest National Laboratory.

https://doi.org/10.5194/egusphere-2025-4910
Preprint. Discussion started: 13 November 2025

REFERENCES

Adler, R. F., Huffman, G. J., Chang, A., Ferraro, R., Xie, P. P., Janowiak, J., Rudolf, B., Schneider, U., Curtis, S., Bolvin, D., Gruber, A., Susskind, J., Arkin, P., and Nelkin, E.: The version-2 Global Precipitation Climatology Project (GPCP) monthly precipitation analysis (1979–present), Journal of Hydrometeorology, 4, 1147–1167, https://doi.org/10.1175/1525-7541(2003)004<1147:TVGPCP>2.0.CO;2, 2003.

Boer, G. J., Smith, D. M., Cassou, C., Doblas-Reyes, F., Danabasoglu, G., Kirtman, B., Kushnir, Y., Kimoto, M., Meehl, G. A., Msadek, R., Mueller, W. A., Taylor, K. E., Zwiers, F., Rixen, M., Ruprich-Robert, Y., and Eade, R.: The Decadal Climate Prediction Project (DCPP) contribution to CMIP6, Geoscientific Model Development, 9, 3751–3777, https://doi.org/10.5194/gmd-9-3751-2016, 2016.

Browne, P. A., De Rosnay, P., Zuo, H., Bennett, A. and Dawson, A.: Weakly coupled ocean–atmosphere data assimilation in the ECMWF NWP system, Remote Sensing, 11, 234, https://doi.org/10.3390/rs11030234, 2019.

Carton, J. A. and Giese, B. S.: A reanalysis of ocean climate using Simple Ocean Data Assimilation (SODA), Monthly Weather Review, 136, 2999–3017, https://doi.org/10.1175/2007MWR1978.1, 2008.

Chiang, J. C. H. and Sobel, A. H.: Tropical tropospheric temperature variations caused by ENSO and their influence on the remote tropical climate, Journal of Climate, 15, 2616–2631, https://doi.org/10.1175/1520-0442(2002)015<2616:TTTVCB>2.0.CO;2, 2002.

Craig, A. P., Vertenstein, M. and Jacob, R.: A new flexible coupler for Earth system modeling developed for CCSM4 and CESM1, The International Journal of High Performance Computing Applications, 26, 31–42, https://doi.org/10.1177/1094342011428141, 2012.

Doblas-Reyes, F. J., Andreu-Burillo, I., Chikamoto, Y., García-Serrano, J., Guemas, V., Kimoto, M., Mochizuki, T., Rodrigues, L. R. L., and van Oldenborgh, G. J.: Initialized near-term regional climate change prediction, Nature Communications, 4, 1715, https://doi.org/10.1038/ncomms2704, 2013.

Enfield, D. B., Mestas-Nuñez, A. M. and Trimble, P. J.: The Atlantic Multidecadal Oscillation and its relation to rainfall and river flows in the continental U.S., Geophysical Research

https://doi.org/10.5194/egusphere-2025-4910
Preprint. Discussion started: 13 November 2025

Letters, 28, 2077–2080, https://doi.org/10.1029/2000GL012745, 2001.

Eyring, V., Bony, S., Meehl, G. A., Senior, C. A., Stevens, B., Stouffer, R. J. and Taylor, K. E.: Overview of the Coupled Model Intercomparison Project Phase 6 (CMIP6) experimental design and organization, Geoscientific Model Development, 9, 1937–1958, https://doi.org/10.5194/gmd-9-1937-2016, 2016.

Feng, X., Haines, K. and de Boisséson, E.: Coupling of surface air and sea surface temperatures in the CERA-20C reanalysis, Quarterly Journal of the Royal Meteorological Society, 144, 195–207, https://doi.org/10.1002/qj.3194, 2018.

Golaz, J. C., Caldwell, P. M., Van Roekel, L. P., Petersen, M. R., Tang, Q., Wolfe, J. D., Abeshu, G., Anantharaj, V., Asay-Davis, X. S., Bader, D. C., Baldwin, S. A., Bisht, G., Bogenschutz, P. A., Branstetter, M., Brunke, M. A., Brus, S. R., Burrows, S. M., Cameron-Smith, P. J., Donahue, A. S., Deakin, M., Easter, R. C., Evans, K. J., Feng, Y., Flanner, M., Foucar, J. G., Fyke, J. G., Griffin, B. M., Hannay, C., Harrop, B. E., Hoffman, M. J., Hunke, E. C., Jacob, R. L., Jacobsen, D. W., Jeffery, N., Jones, P. W., Keen, N. D., Klein, S. A., Larson, V. E., Leung, L. R., Li, H. Y., Lin, W., Lipscomb, W. H., Ma, P. L., Mahajan, S., Maltrud, M. E., Mametjanov, A., McClean, J. L., McCoy, R. B., Neale, R. B., Price, S. F., Qian, Y., Rasch, P. J., Reeves Eyre, J. E. J., Riley, W. J., Ringler, T. D., Roberts, A. F., Roesler, E. L., Salinger, A. G., Shaheen, Z., Shi, X., Singh, B., Tang, J., Taylor, M. A., Thornton, P. E., Turner, A. K., Veneziani, M., Wan, H., Wang, H., Wang, S., Williams, D. N., Wolfram, P. J., Worley, P. H., Xie, S., Yang, Y., Yoon, J.-H., Zelinka, M. D., Zender, C. S., Zeng, X., Zhang, C., Zhang, K., Zhang, Y., Zheng, X., Zhou, T., and Zhu, Q.: The DOE E3SM Coupled Model Version 1: Overview and Evaluation at Standard Resolution, Journal of Advances in Modeling Earth Systems, 11, 2089–2129, https://doi.org/https://doi.org/10.1029/2018MS001603, 2019.

Golaz, J. C., Van Roekel, L. P., Zheng, X., Roberts, A. F., Wolfe, J. D., Lin, W. Y., Bradley, A. M., Tang, Q., Maltrud, M. E., Forsyth, R. M., Zhang, C. Z., Zhou, T., Zhang, K., Zender, C. S., Wu, M. X., Wang, H. L., Turner, A. K., Singh, B., Richter, J. H., Qin, Y., Petersen, M. R., Mametjanov, A., Ma, P., Larson, V. E., Krishna, J., Keen, N. D., Jeffery, N., Hunke, E. C., Hannah, W. M., Guba, O., Griffin, B. M., Feng, Y., Engwirda, D., Vittorio, A. V., Cheng, D., Conlon, L. M., Chen, C., Brunke, M. A., Bisht, G., Benedict, J. J., Asay-Davis, X. S., Zhang, Y. Y., Zhang, M., Zeng, X. B., Xie, S. C., Wolfram, P. J., Vo, T., Veneziani, M., Tesfa, T. K., Sreepathi, S., Salinger, A. G., Jack Reeves Eyre, J. E., Prather, M. J., Mahajan, S., Li, Q., Jones, P. W., Jacob, R. L., Huebler, G. W., Huang, X. L., Hillman, B. R., Harrop, B. E., Foucar, J. G., Fang, Y. L., Comeau, D. S., Caldwell, P. M., Bartoletti, T., Balaguru, K., Taylor, M. A., McCoy, R. B., Leung, L. R., and Bader, D. C.: The DOE E3SM Model version 2: Overview of the physical model and initial model evaluation, Journal of Advances in Modeling Earth Systems, 14, e2022MS003156, https://doi.org/10.1029/2022MS003156, 2022.

Good, S. A., Martin, M. J., and Rayner, N. A.: EN4: Quality controlled ocean temperature and salinity profiles and monthly objective analyses with uncertainty estimates, Journal of Geophysical Research: Oceans, 118(12), 6704–6716, https://doi.org/10.1002/2013JC009067, 2013.

Han, G., Wu, X., Zhang, S., Liu, Z. and Li, W.: Error covariance estimation for coupled data assimilation using a Lorenz atmosphere and a simple pycnocline ocean model, Journal of Climate, 26, 10218–10231, https://doi.org/10.1175/JCLI-D-13-00236.1, 2013.

Hanley, D. E., Bourassa, M. A., O'Brien, J. J., Smith, S. R. and Spade, E. R.: A quantitative evaluation of ENSO indices, Journal of Climate, 16, 1249–1258, https://doi.org/10.1175/1520-0442(2003)16<1249:AQEOEI>2.0.CO;2, 2003.

Hersbach, H., Bell, B., Berrisford, P., Hirahara, S., Horányi, A., Muñoz-Sabater, J., Nicolas, J., Peubey, C., Radu, R., Schepers, D., Simmons, A., Soci, C., Abdalla, S., Abellan, X., Balsamo, G., Bechtold, P., Biavati, G., Bidlot, J., Bonavita, M., De Chiara, G., Dahlgren, P., Dee, D., Diamantakis, M., Dragani, R., Flemming, J., Forbes, R., Fuentes, M., Geer, A., Haimberger, L., Healy, S., Hogan, R. J., Hólm, E., Janisková, M., Keeley, S., Laloyaux, P., Lopez, P., Lupu, C., Radnoti, G., de Rosnay, P., Rozum, I., Vamborg, F., Villaume, S., and Thépaut, J.-N.: The ERA5 global reanalysis, Quarterly Journal of the Royal Meteorological Society, 146, 1999–2049, https://doi.org/10.1002/qj.3803, 2020.

He, Y., Wang, B., Huang, W., Xu, S., Wang, Y., Liu, L., Li, L., Liu, J., Yu, Y., Lin, Y., Huang, X., and Peng, Y.: A new DRP-4DVar-based coupled data assimilation system for decadal

https://doi.org/10.5194/egusphere-2025-4910
Preprint. Discussion started: 13 November 2025

predictions using a fast online localization technique, Climate Dynamics, 54, 3541–3559, https://doi.org/10.1007/s00382-020-05190-w, 2020.

Higgins, R. W., Leetmaa, A., Xue, Y. and Barnston, A.: Dominant factors influencing the seasonal predictability of U.S. precipitation and surface air temperature, Journal of Climate, 13, 3994–4017, https://doi.org/10.1175/1520-0442(2000)013<3994:DFITSP>2.0.CO;2, 2000.

Ju, X., Chen, S., Chen, W., Wu, R., Chen, L. and Cheng, X.: Origins of the overestimated Indian Ocean Dipole amplitude in current coupled climate models, Climate Dynamics, 63, 180, https://doi.org/10.1007/s00382-025-07673-0, 2025.

Leung, L. R., Bader, D. C., Taylor, M. A. and McCoy, R. B.: An introduction to the E3SM special collection: Goals, science drivers, development, and analysis, Journal of Advances in Modeling Earth Systems, 12, e2019MS001821, https://doi.org/10.1029/2019MS001821, 2020.

Li, H., Wigmosta, M. S., Wu, H., Huang, M., Ke, Y., Coleman, A. M. and Leung, L. R.: A physically based runoff routing model for land surface and Earth system models, Journal of Hydrometeorology, 14, 808–828, https://doi.org/10.1175/JHM-D-12-015.1, 2013.

Lin, L. F. and Pu, Z.: Examining the impact of SMAP soil moisture retrievals on short-range weather prediction under weakly and strongly coupled data assimilation with WRF-Noah, Monthly Weather Review, 147, 4345–4366, https://doi.org/10.1175/MWR-D-19-0017.1, 2019.

Lin, L. F. and Pu, Z.: Improving near-surface short-range weather forecasts using strongly coupled land–atmosphere data assimilation with GSI-EnKF, Monthly Weather Review, 148, 2863-2888, https://doi.org/10.1175/MWR-D-19-0370.1, 2020.

Liu, J., Wang, B. and Xiao, Q.: An evaluation study of the DRP-4DVar approach with the Lorenz-96 model, Tellus A: Dynamic Meteorology and Oceanography, 63, 256–262, https://doi.org/10.1111/j.1600-0870.2010.00487.x, 2011.

Mantua, N. J., Hare, S. R., Zhang, Y., Wallace, J. M. and Francis, R. C.: A Pacific interdecadal climate oscillation with impacts on salmon production, Bulletin of the American Meteorological Society, 78, 1069–1080, https://doi.org/10.1175/1520-

https://doi.org/10.5194/egusphere-2025-4910
Preprint. Discussion started: 13 November 2025

0477(1997)078<1069:APICOW>2.0.CO;2, 1997.

Meehl, G. A., Richter, J. H., Teng, H., Capotondi, A., Cobb, K., Doblas-Reyes, F., Donat, M. G., England, M. H., Fyfe, J. C., Han, W., Kim, H., Kirtman, B. P., Kushnir, Y., Lovenduski, N. S., Mann, M. E., Merryfield, W. J., Nieves, V., Pegion, K., Rosenbloom, N., Sanchez, S. C., Scaife, A. A., Smith, D., Subramanian, A. C., Sun, L., Thompson, D., Ummenhofer, C. C., and Xie, S.-P.: Initialized Earth system prediction from subseasonal to decadal timescales, Nature Reviews Earth & Environment, 2, 340–357, https://doi.org/10.1038/s43017-021-00155-x, 2021.

Mulholland, D. P., Laloyaux, P., Haines, K. and Balmaseda, M. A.: Origin and impact of initialization shocks in coupled atmosphere–ocean forecasts, Monthly Weather Review, 143, 4631–4644, https://doi.org/10.1175/MWR-D-15-0076.1, 2015.

Penny, S. G., Bach, E., Bhargava, K., Chang, C.-C., Da, C., Sun, L. and Yoshida, T.: Strongly coupled data assimilation in multiscale media: Experiments using a quasi-geostrophic coupled model, Journal of Advances in Modeling Earth Systems, 11, 1803–1829, https://doi.org/10.1029/2019MS001652, 2019.

Rayner, N. A., Parker, D. E., Horton, E. B., Folland, C. K., Alexander, L. V., Rowell, D. P., Kent, E. C. and Kaplan, A.: Global analyses of sea surface temperature, sea ice, and night marine air temperature since the late nineteenth century, Journal of Geophysical Research: Atmospheres, 108, 4407, https://doi.org/10.1029/2002JD002670, 2003.

Reckinger, S. M., Petersen, M. R. and Reckinger, S. J.: A study of overflow simulations using MPAS-Ocean: Vertical grids, resolution, and viscosity, Ocean Modelling, 96, 291–313, https://doi.org/10.1016/j.ocemod.2015.09.006, 2015.

Ropelewski, C. F. and Halpert, M. S.: North American precipitation and temperature patterns associated with the El Niño/Southern Oscillation (ENSO), Monthly Weather Review, 114, 2352–2362, https://doi.org/10.1175/1520-0493(1986)114<2352:NAPATP>2.0.CO;2, 1986.

Saji, N. H., Goswami, B. N., Vinayachandran, P. N. and Yamagata, T.: A dipole mode in the tropical Indian Ocean, Nature, 401, 360–363, https://doi.org/10.1038/43854, 1999.

Saji, N. H., Xie, S.-P. and Yamagata, T.: Tropical Indian Ocean variability in the IPCC twentieth-century climate simulations, Journal of Climate, 19, 4397–4417, https://doi.org/10.1175/JCLI3847.1, 2006.

Shi, P., Lu, H., Leung, L.R., He, Y., Wang, B., Yang, K., Yu, L., Liu, L., Huang, W., Xu, S., Liu, J., Huang, X., Li, L., and Lin, Y.: Significant land contributions to interannual predictability of East Asian summer monsoon rainfall, Earth's Future, 9(2), e2020EF001762, https://doi.org/10.1029/2020EF001762, 2021.

Shi, P., Wang, B., He, Y., Lu, H., Yang, K., Xu, S. M., Huang, W. Y., Liu, L., Liu, J. J., Li, L. J., and Wang, Y.: Contributions of weakly coupled data assimilation–based land initialization to interannual predictability of summer climate over Europe, Journal of Climate, 35, 517–535, https://doi.org/10.1175/JCLI-D-20-0506.1, 2022.

Shi, P., Leung, L. R., Wang, B., Zhang, K., Hagos, S. M. and Zhang, S.: The 4DEnVar-based weakly coupled land data assimilation system for E3SM version 2, Geoscientific Model Development, 17, 3025–3040, https://doi.org/10.5194/gmd-17-3025-2024, 2024a.

Shi, P., Leung, L. R., Lu, H., Wang, B., Yang, K. and Chen, H.: Uncovering the interannual predictability of the 2003 European summer heatwave linked to the Tibetan Plateau, npj Climate and Atmospheric Science, 7, 242, https://doi.org/10.1038/s41612-024-00782-3, 2024b.

Shi, P., Leung, L. R. and Wang, B.: Development and evaluation of a new 4DEnVar-based weakly coupled ocean data assimilation system in E3SMv2, Geoscientific Model Development, 18, 2443–2460, https://doi.org/10.5194/gmd-18-2443-2025, 2025.

Sluka, T. C., Penny, S. G., Kalnay, E. and Miyoshi, T.: Assimilating atmospheric observations into the ocean using strongly coupled ensemble data assimilation, Geophysical Research Letters, 43, 752–759, https://doi.org/10.1002/2015GL067238, 2016.

Tang, Q., Mu, L., Goessling, H. F., Semmler, T. and Nerger, L.: Strongly coupled data assimilation of ocean observations into an ocean-atmosphere model, Geophysical Research Letters, 48, e2021GL094941, https://doi.org/10.1029/2021GL094941, 2021.

Taylor, K. E., Stouffer, R. J. and Meehl, G. A.: An overview of CMIP5 and the experiment design, Bulletin of the American Meteorological Society, 93, 485–498, https://doi.org/10.1175/BAMS-D-11-00094.1, 2012.

https://doi.org/10.5194/egusphere-2025-4910
Preprint. Discussion started: 13 November 2025

Trenberth, K. E. and Stepaniak, D. P.: Indices of El Niño evolution, Journal of Climate, 14, 1697–1701, https://doi.org/10.1175/1520-0442(2001)014<1697:LIOENO>2.0.CO;2, 2001.

Turner, A. K., Lipscomb, W. H., Hunke, E. C., Jacobsen, D. W., Jeffery, N., Engwirda, D., Ringler, T. D. and Wolfe, J. D.: MPAS-Seaice (v1.0.0): Sea-ice dynamics on unstructured Voronoi meshes, Geoscientific Model Development, 15, 3721–3751, https://doi.org/10.5194/gmd-15-3721-2022, 2022.

Wang, B., Liu, J., Wang, S., Cheng, W., Liu, J., Liu, C., Xiao, Q., and Kuo, Y. H.: An economical approach to four-dimensional variational data assimilation, Advances in Atmospheric Sciences, 27, 715–727, https://doi.org/10.1007/s00376-009-9122-3, 2010.

Wang, C.: Three-ocean interactions and climate variability: A review and perspective, Climate Dynamics, 53, 5119–5136, https://doi.org/10.1007/s00382-019-04930-x, 2019.

Wu, B., Zhou, T. and Zheng, F.: EnOI-IAU initialization scheme designed for decadal climate prediction system IAP-DecPreS, Journal of Advances in Modeling Earth Systems, 10, 342–356, https://doi.org/10.1002/2017MS001132, 2018.

Zhang, S.: A study of impacts of coupled model initial shocks and state–parameter optimization on climate predictions using a simple pycnocline prediction model, Journal of Climate, 24, 6210–6226, https://doi.org/10.1175/JCLI-D-10-05003.1, 2011.

Zhang, S., Liu, Z., Rosati, A. and Delworth, T.: A study of enhancive parameter correction with coupled data assimilation for climate estimation and prediction using a simple coupled model, Tellus A: Dynamic Meteorology and Oceanography, 64, 10963, https://doi.org/10.3402/tellusa.v64i0.10963, 2012.

Zhang, S., Liu, Z., Zhang, X., Wu, X., Han, G., Zhao, Y., et al.: Coupled data assimilation and parameter estimation in coupled ocean–atmosphere models: A review, Climate Dynamics, 54, 5127–5144, https://doi.org/10.1007/s00382-020-05275-6, 2020.

Zhou, W., Li, J., Yan, Z., Shen, Z., Wu, B., Wang, B., Zhang, R., and Li, Z.: Progress and future prospects of decadal prediction and data assimilation: A review, Atmospheric and Oceanic Science Letters, 17, 100441, https://doi.org/10.1016/j.aosl.2023.100441, 2024.

Zhu, J., Kumar, A., Lee, H.-C. and Wang, H.: Seasonal predictions using a simple ocean

https://doi.org/10.5194/egusphere-2025-4910
Preprint. Discussion started: 13 November 2025

initialization scheme, Climate Dynamics, 49, 3989–4007, https://doi.org/10.1007/s00382-017-3556-6, 2017.

Zhu, S., Wang, B., Zhang, L., Liu, J., Liu, Y., Gong, J., Xu, S., Wang, Y., Huang, W., Liu, L., He, Y., and Wu, X.: A Four-Dimensional Ensemble-Variational (4DEnVar) Data Assimilation System Based on GRAPES-GFS: System Description and Primary Tests, Journal of Advances in Modeling Earth Systems, 14(7), e2021MS002737, https://doi.org/10.1029/2021MS002737, 2022.

https://doi.org/10.5194/egusphere-2025-4910
Preprint. Discussion started: 13 November 2025

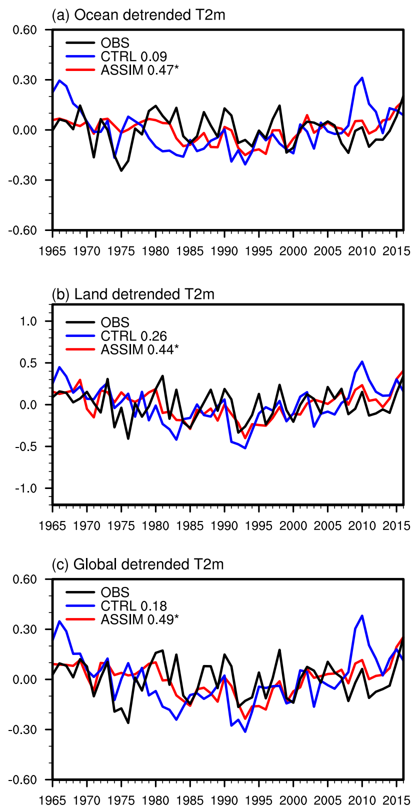

Figure 1. Time series of detrended annual mean surface air temperature anomalies (units: °C) over (a) ocean, (b) land, and (c) global domains from 1965 to 2016. Black line: observation; blue line: CTRL; red line: ASSIM. Temperature anomalies are computed by removing both the climatological mean and long-term trend. The correlation coefficients of CTRL and ASSIM with the observation are also shown. The asterisk denotes statistically significant correlation at the 95% confidence level.

https://doi.org/10.5194/egusphere-2025-4910
Preprint. Discussion started: 13 November 2025

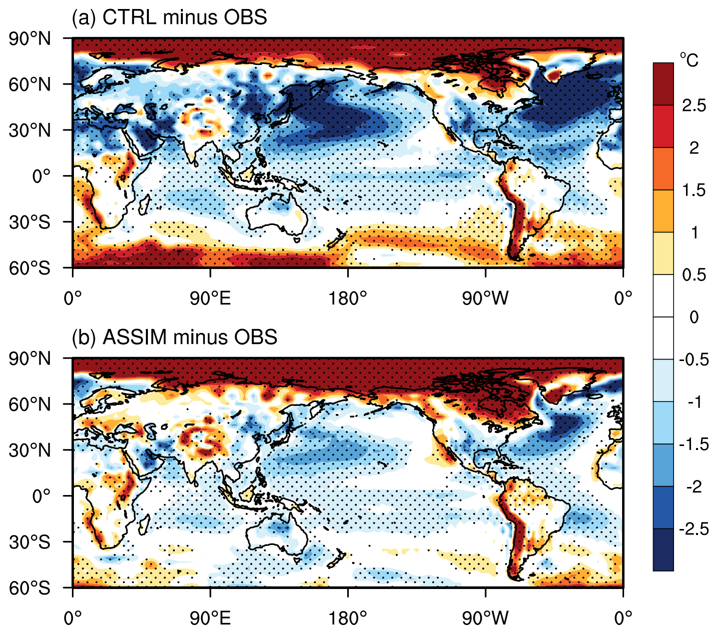

Figure 2. Spatial patterns of climatological mean differences in surface air temperature (units: °C) between model simulations and observations for the period 1965–2016. Panel (a) shows the difference between CTRL and observation, and panel (b) shows the difference between ASSIM and observation. Dotted areas denote regions where the differences are statistically significant at the 95% confidence level.

https://doi.org/10.5194/egusphere-2025-4910
Preprint. Discussion started: 13 November 2025

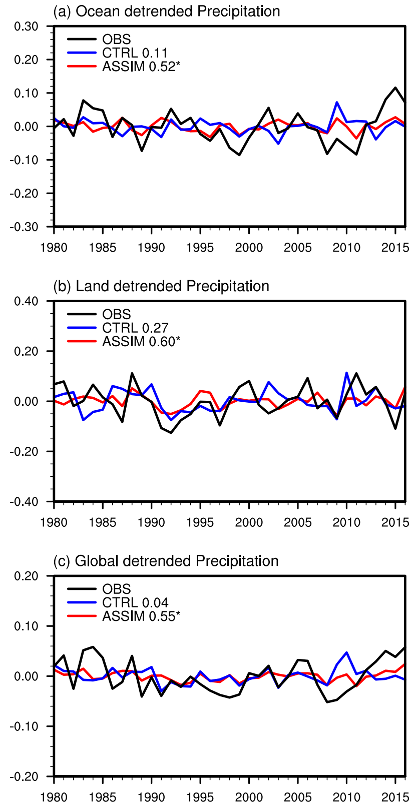

Figure 3. Time series of detrended annual mean precipitation anomalies (units: mm day^{-1}) over (a) ocean, (b) land, and (c) global domains from 1980 to 2016. Black line: observation; blue line: CTRL; red line: ASSIM. Precipitation anomalies are computed by removing both the climatological mean and long-term trend. The correlation coefficients of CTRL and ASSIM with the observation are also shown. The asterisk denotes statistically significant correlation at the 95% confidence level.

https://doi.org/10.5194/egusphere-2025-4910
Preprint. Discussion started: 13 November 2025

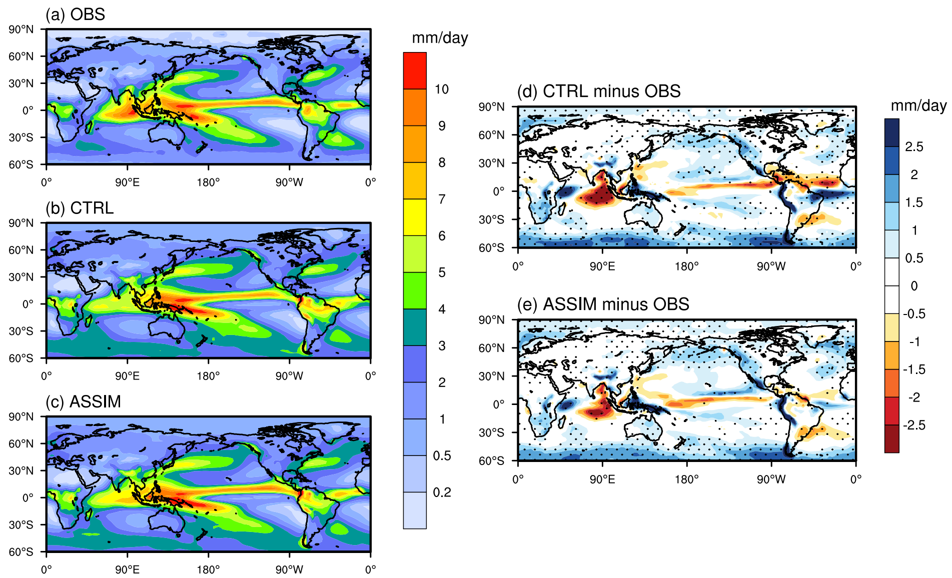

Figure 4. Spatial patterns of (a–c) climatological mean precipitation (units: mm day^{-1}) and (d, e) precipitation differences for the period 1980–2016. Panels (a–c) show precipitation climatology from observation, CTRL, and ASSIM, respectively. Panels (d, e) represent precipitation differences between model simulations and observations: (d) CTRL minus observation and (e) ASSIM minus observation. Dotted areas indicate regions where the differences are statistically significant at the 95% confidence level.

https://doi.org/10.5194/egusphere-2025-4910
Preprint. Discussion started: 13 November 2025

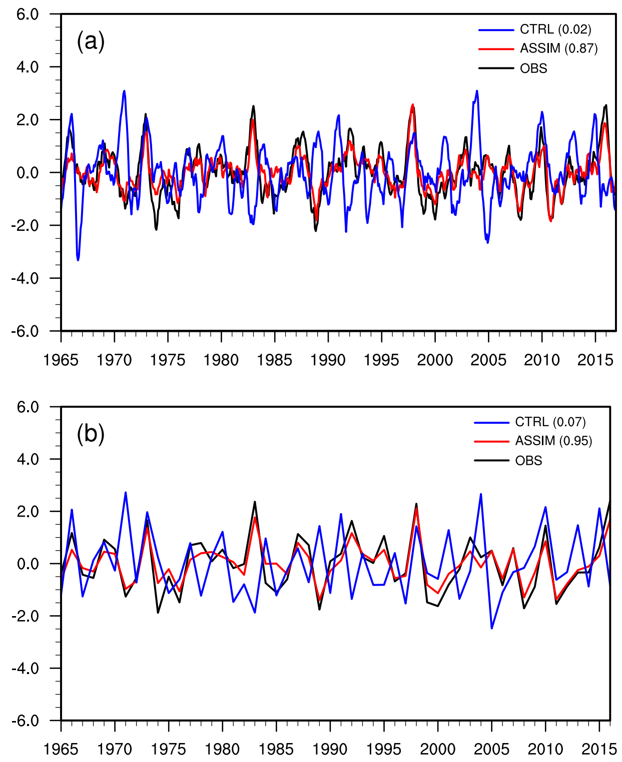

Figure 5. Time series of the (a) monthly and (b) winter Niño 3.4 index from 1965 to 2016 for the observation (black line), ASSIM (red line), and CTRL (blue line). The correlation coefficients with the observation for ASSIM and CTRL are also shown in parentheses.

https://doi.org/10.5194/egusphere-2025-4910
Preprint. Discussion started: 13 November 2025

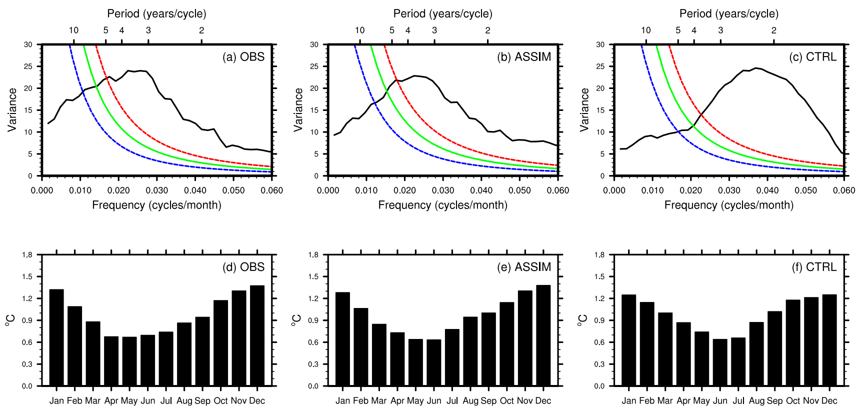

Figure 6. Power spectra (a–c) and seasonal cycle of the standard deviation (d–f) of the monthly Niño 3.4 index from the observation (left column), ASSIM (middle column), and CTRL (right column) for the period 1965–2016. The theoretical Markov "red noise" spectrum is shown as a solid green line, with the 5% and 95% confidence bounds indicated by dashed blue and red lines, respectively.

https://doi.org/10.5194/egusphere-2025-4910
Preprint. Discussion started: 13 November 2025

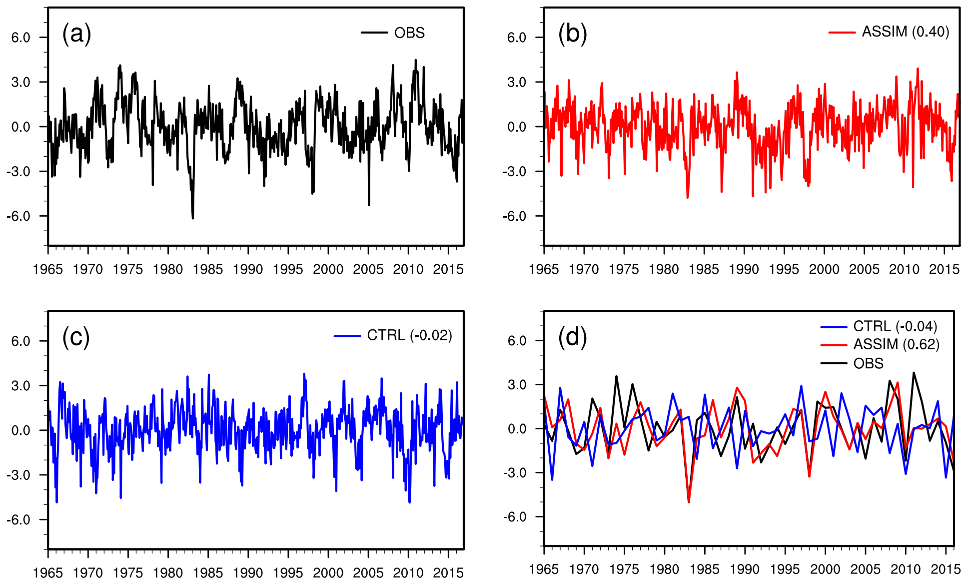

Figure 7. Time series of the (a–c) monthly and (d) winter Southern Oscillation Index (SOI) from 1965 to 2016 for the observation (black line), ASSIM (red line), and CTRL (blue line). Panels (a–c) show individual monthly time series from OBS, ASSIM, and CTRL, respectively, while panel (d) shows the winter SOI averaged over December–February (DJF). The correlation coefficients with the observation in ASSIM and CTRL are also indicated in parentheses.

https://doi.org/10.5194/egusphere-2025-4910
Preprint. Discussion started: 13 November 2025

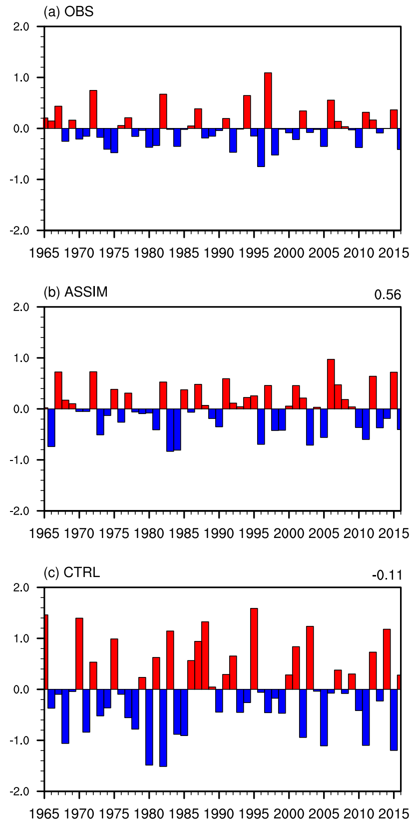

Figure 8. Time series of the autumn (September–November) Dipole Mode Index (DMI) from 1965 to 2016 for (a) the observation, (b) ASSIM, and (c) CTRL. The correlation coefficients of ASSIM and CTRL with the observed DMI are also shown in the upper-right corner.

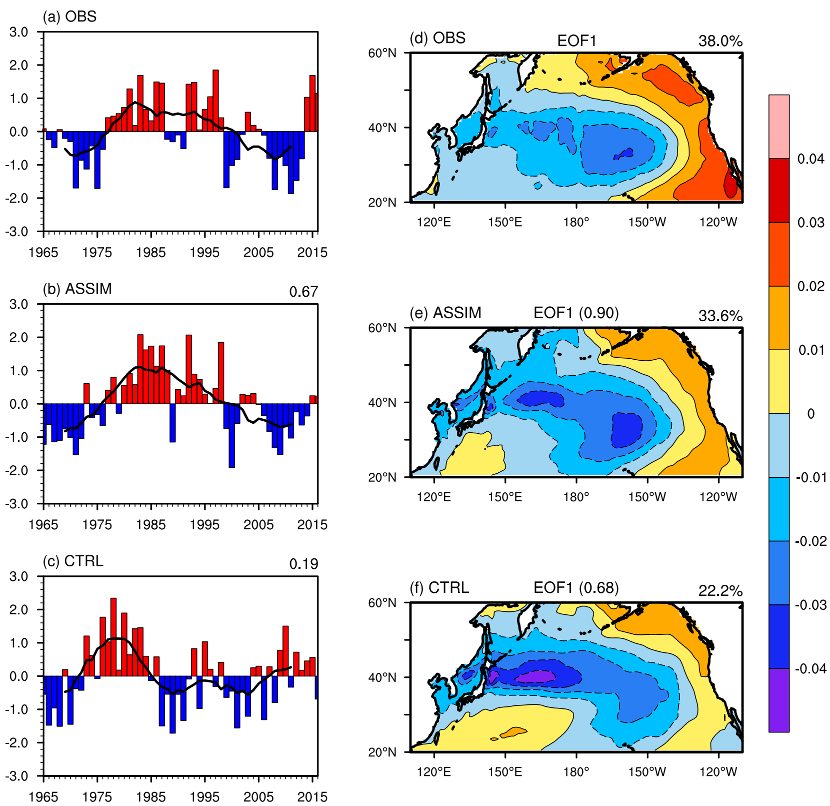

Figure 9. Time series and spatial patterns of the Pacific Decadal Oscillation (PDO) index from 1965 to 2016 for (a, d) the observation, (b, e) ASSIM, and (c, f) CTRL. The black lines in panels (a–c) denote the 10-year running mean of the annual PDO index. The numbers at the top right of (b) and (c) indicate the temporal correlations of ASSIM and CTRL with observations. The percentage of variance explained by EOF1 is shown at the top right of (d–f), and the numbers at the top center of (e) and (f) indicate the spatial correlations with the observed pattern.

https://doi.org/10.5194/egusphere-2025-4910
Preprint. Discussion started: 13 November 2025

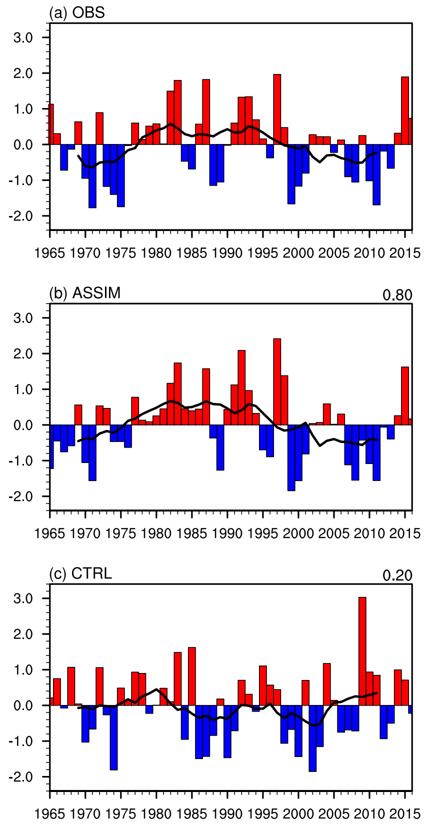

Figure 10. Time series of the Interdecadal Pacific Oscillation (IPO) index from 1965 to 2016 for (a) the observation, (b) ASSIM, and (c) CTRL. The black line in each panel denotes the 10-year running mean of the annual IPO index. The numbers at the top right of (b) and (c) indicate the temporal correlations of ASSIM and CTRL with observations.

https://doi.org/10.5194/egusphere-2025-4910
Preprint. Discussion started: 13 November 2025

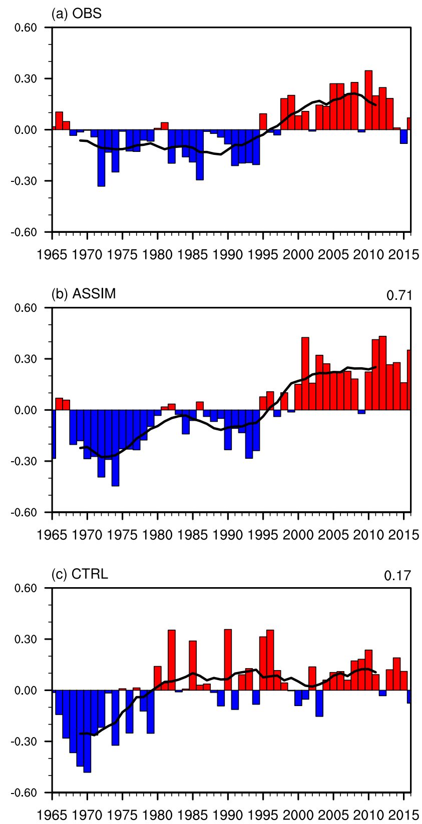

Figure 11. Time series of the Atlantic Multidecadal Oscillation (AMO) index from 1965 to 2016 for (a) the observation, (b) ASSIM, and (c) CTRL. The black line denotes the 10-year running mean. The numbers at the top right of (b) and (c) indicate the temporal correlations of ASSIM and CTRL with observations.

https://doi.org/10.5194/egusphere-2025-4910
Preprint. Discussion started: 13 November 2025

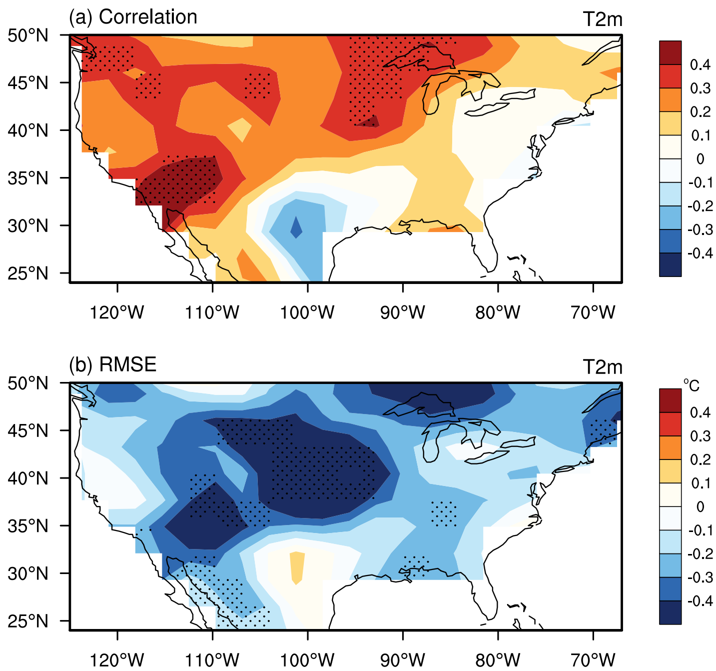

Figure 12. Spatial patterns of the differences in (a) correlation coefficients and (b) root-mean-square errors (RMSE; °C) of detrended winter surface air temperature anomalies between ASSIM and CTRL with observations from 1980 to 2016 over the contiguous U.S. Dotted areas indicate regions where the differences are statistically significant at the 90% confidence level.

https://doi.org/10.5194/egusphere-2025-4910
Preprint. Discussion started: 13 November 2025

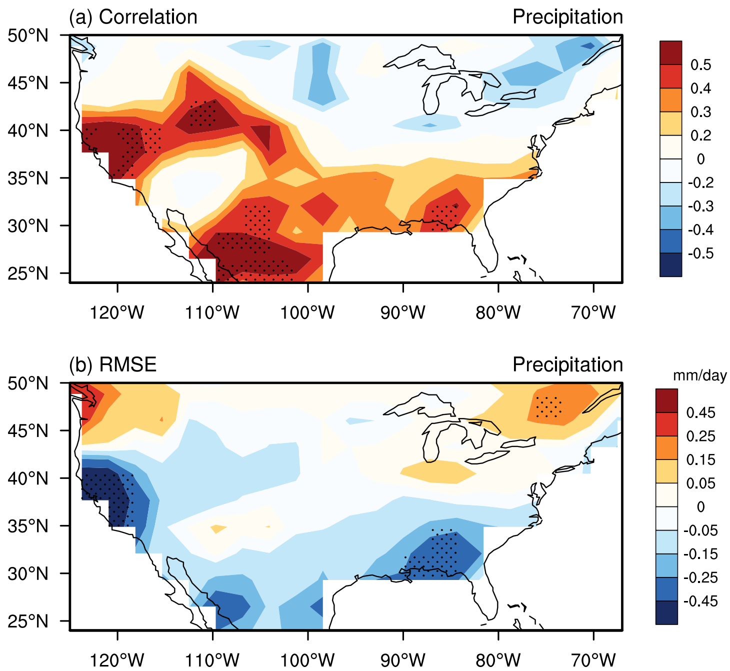

719

720 **Figure 13.** Similar to Fig. 12 but for detrended winter precipitation.

https://doi.org/10.5194/egusphere-2025-4910
Preprint. Discussion started: 13 November 2025

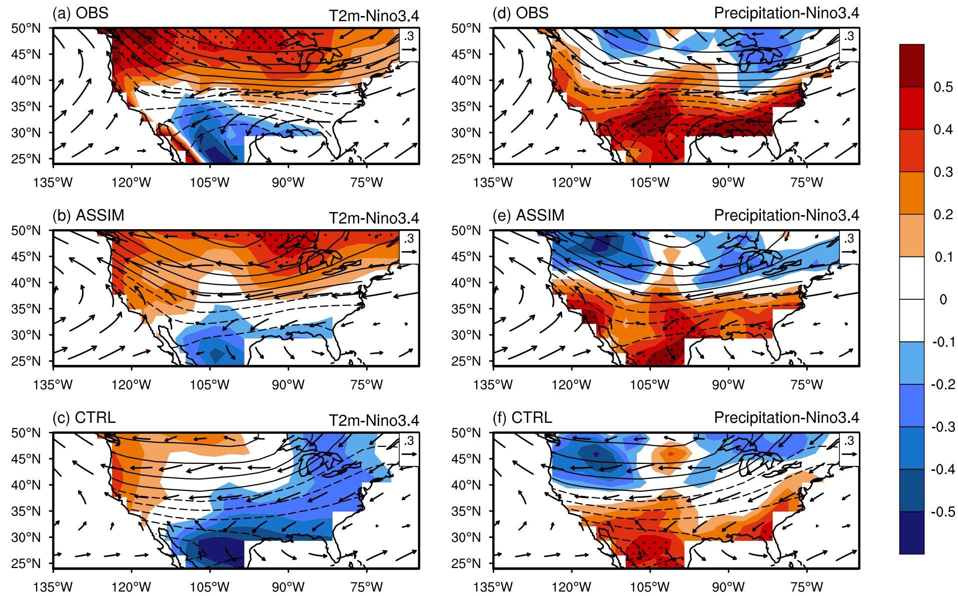

Figure 14. Regression patterns of winter surface air temperature (left column; shaded) and precipitation (right column; shaded), 500hPa geopotential height (contours), and 850hPa winds (vectors) on the standardized Niño 3.4 index for (a, d) the observation, (b, e) ASSIM, and (c, f) CTRL. Dotted areas indicate regions where the regressions are statistically significant at the 95% confidence level.